Mine Water and the Environment (2023) 42:560–577
https://doi.org/10.1007/s10230-023-00956-0

TECHNICAL ARTICLE

Role of Secondary Sulfate Minerals on Metal Recycling in an Abandoned Copper Deposit: Kuvarshan (Artvin), Northeastern Turkey

I. Yolcubal[1] · A. Doğrul Demiray[2] · E. Çiftçi[1] · E. Sangu[2]

Received: 27 January 2023 / Accepted: 26 October 2023 / Published online: 22 November 2023

Abstract
Mine tailings left at abandoned sulfide mine sites can seriously threaten surrounding ecosystems and cause soil and water pollution. This study focused on determining the geochemical processes and mineral phases controlling metal cycling in an abandoned copper mine site (Kuvarshan, Artvin, northeastern Turkey). Geochemical and mineralogical characterization studies were conducted to determine the chemical and mineral compositions of the tailings, leachates, and AMD products. In addition, kinetic tests and geochemical modeling studies were performed on the tailings to evaluate the rates and mechanisms of metal release. Oxidation of pyrite in the tailings played an important role in the formation of acidic mine drainages (pH ≈ 2.7–3.1) with high sulfate and metal contents. Sequestration of Fe and As in the AMD was controlled by jarosite precipitation. A large fraction of the total Fe (73%) and As (98%) remained in the suspended phase in the acidic water. Furthermore, the local precipitation of aragonite from alkaline mine leachates also removed zinc, copper, arsenic, and lead ions from the solution, and minimized the release of these metals into the environment. On the other hand, dissolution of secondary sulfate mineral precipitates (i.e. chalcoalumite, chalcocyanite, goslarite, coquimbite, and rozenite) contributed to the enrichment of Al, Cu, Fe, Zn, As, and Pb in the mine leachates and metal loading into a nearby stream during the wet period.

Keywords Acid mine drainage · Humidity cell experiment · Heavy metals · Jarosite · Efflorescent sulfate salts

Introduction

Mine tailings left behind at abandoned sulfide mine sites pose a significant and ongoing threat to the surrounding ecosystems (Dold 2014). The process of sulfide mineral oxidation in tailings can lead to the formation of highly acidic mine drainage (AMD) that contain elevated levels of metals and total dissolved solids (Nordstrom and Alpers 1999), resulting in the contamination of surface water and groundwater resources (Lapakko 2002; Lottermoser 2007; Nordstrom 1982; Singer and Stumm 1970).

Assessing the environmental risks associated with these mine wastes and developing strategies for rehabilitation of the abandoned mine sites require a detailed geochemical and mineralogical characterization of the tailings and determination of the geochemical processes and secondary mineral phases controlling AMD formation and sequestration or release of metals into the soil and aqueous environment (Dold 2014; Jacobs et al. 2014; Jambor et al. 2000; Lapakko 2002; Miller et al. 2009).

This study was focused on determining the geochemical processes and mineral phases controlling the formation of AMD and metal cycling in the abandoned Kuvarshan mine site located in the eastern Black Sea Region of Turkey. This was done via detailed geochemical and mineralogical characterization of the tailings, AMD precipitates, and mine leachates, characterization of the elution chemistry in kinetic tests (humidity cell tests), and geochemical modeling.

The eastern Black Sea Region of Turkey hosts many polymetallic mines and is one of the regions in Turkey with the greatest potential for environmental problems from the exploitation of such deposits, as it is a region where volcanogenic massive sulfide (VMS) deposits are concentrated and operated intensively. According to the inventory of the

✉ I. Yolcubal
yolcubal@itu.edu.tr

[1] Department of Geological Engineering, Istanbul Technical University, Faculty of Mines, 34469 Istanbul, Turkey

[2] Department of Geological Eng, Kocaeli University, 41380 Kocaeli, Turkey

General Directorate of Mineral Exploration and Research (MTA, Turkey), there are a total of 72 metallic mine sites in Artvin Province, 44 of which are copper–lead–zinc, one iron, 17 manganese, five copper-molybdenum, and five gold deposits and exposures.

The Kuvarshan copper mine, which was chosen as the pilot study area, is situated ≈ 2 km northeast of the Artvin Province Kuvarshan (Bakırköy) village in the northeastern part of Turkey (Fig. 1). The Kuvarshan deposit resembles many aspects of the other Kuroko-type VMS deposits found in the eastern Pontide, such as mineral paragenesis, wall-rock, S-isotope characteristics, and ore mineral chemistry (Çiftçi et al. 2009). Currently, the Kuvarshan mine site is licensed to Eti Bakır A.Ş., and its operation dates back to before World War I. Historical records from the MTA indicate that ≈ 350,000 metric tons of 4.5% Cu ore were extracted from the Kuvarshan mine during its operation. Underground mining techniques were used for ore extraction, and most of the galleries, except for one, have since collapsed.

The mine site is characterized by the presence of extensive tailings that cover a large area. Specifically, there are two tailings piles extending over ≈ 1 ha (Fig. 1). Additionally, acidic water has accumulated in puddles on the waste rock piles (Fig. 1). Discharges from the mine gallery can also be observed.

The Kuvarshan mine site is situated on the sloping hills within the drainage area of the Fabrika Creek, which flows into the Coruh River (Fig. 1). Climatic and topographical conditions at the site are favorable for oxidation of tailings and the spread of mine leachates to the surrounding drainage networks.

The local climate is characterized as humid continental, with warm summers and a negligible dry season. The average annual precipitation in the Artvin Province is 690 mm, with the highest rainfall occurring in December and January (84–86 mm) and the lowest in July–September (29–38 mm). On average, there are 129 rainy days per year, and the annual average humidity is 74%.

Geology and Paragenesis of the Kuvarshan Copper Mine

The historic Kuvarshan copper mine is located in the Eastern Pontide Metallogenic Belt, which hosts many active and abandoned VMS deposits. Mining began there in 1908 and the mine site has been abandoned since 1941. The geology of the deposit was previously studied in detail by Kraeff (1963) and Simonovic (1972). The Kuvarshan deposit is hosted by Upper Cretaceous dacitic volcanics that are composed of mainly silicified pyritized dacite (Fig. 2). Mineral paragenesis of the mine consisted of chalcopyrite, sphalerite, bornite, chalcocite, and pyrite with minor amounts of tetrahedrite, tennantite, and galena. Quartz, barite, calcite, and gypsum constitute the main gangue minerals. The site is quite rich in pyrite; therefore, the Kuvarshan deposit is also identified as a pyritic Cu-type deposit.

Methods

To determine the mechanisms controlling AMD formation and the kinetics of metal release from tailings at the site, mine tailings (K-15, K-16, K-17), waste rock (WR-3), AMD precipitates (AMD-1p, AMD-2p, AMD-3p), mine leachates (AMD-2, AMD-3), and acidic drainages (AMD-1) were sampled for detailed chemical and mineralogical characterization (Fig. 1). The AMD leachates and precipitates were sampled seasonally, in both dry and wet periods. Leachate samples were taken as both filtered and unfiltered samples. The pH, electrical conductivity (EC), temperature (T), and dissolved oxygen (DO) contents of the samples were measured in situ using a portable multi-parameter meter (Thermo Orion Five Star). Samples were filtered on-site using single-use cellulose acetate syringe filters of 0.45 µm and acidified with supra-pure nitric acid to pH < 2 for metal analyses and kept at 4 ºC in the refrigerator until analyzed. Unfiltered leachate samples were digested with the microwave acid digestion method (EPA 3015A) to determine the total (dissolved plus suspended phases) metal concentrations as well as the metal concentrations adsorbed to the solid phases (EPA 2007).

AMD precipitates occurring on the site were carefully sampled from the bottom of the acidic puddle or the surroundings of the mine leachates with a polyethylene spoon, stored in air-tight plastic containers, and air-dried at ambient temperatures before mineral identification and elemental analysis. Tailings samples (≈ 10 kg) were taken from many randomly selected locations on the waste pile after removing the top 10–20 cm of surface material and were mixed thoroughly to obtain composite samples. Two tailings sites were sampled for mineralogical and geochemical characterization using x-ray fluorescence (XRF, Bruker S8 Tiger wavelength dispersive), x-ray diffraction (XRD, Bruker D8 advance model) analyses, and examination of polished sections, respectively. Loss of ignition (LOI) values of the samples were determined following combustion of the powdered dry sample at 1050 ºC in an ash furnace for 1.5 h. The detection limit for the XRF analysis was 10 mg/kg. XRD measurements were conducted on the fractions of 0.5–10 g (based on sample availability) of the powder samples prepared from the dehumidified samples, ground to < 75 µm, and placed in the sample cup in such a way as to provide random particle orientation, in the XRD Lab of the ITU Geology Department XRD device, with the use of

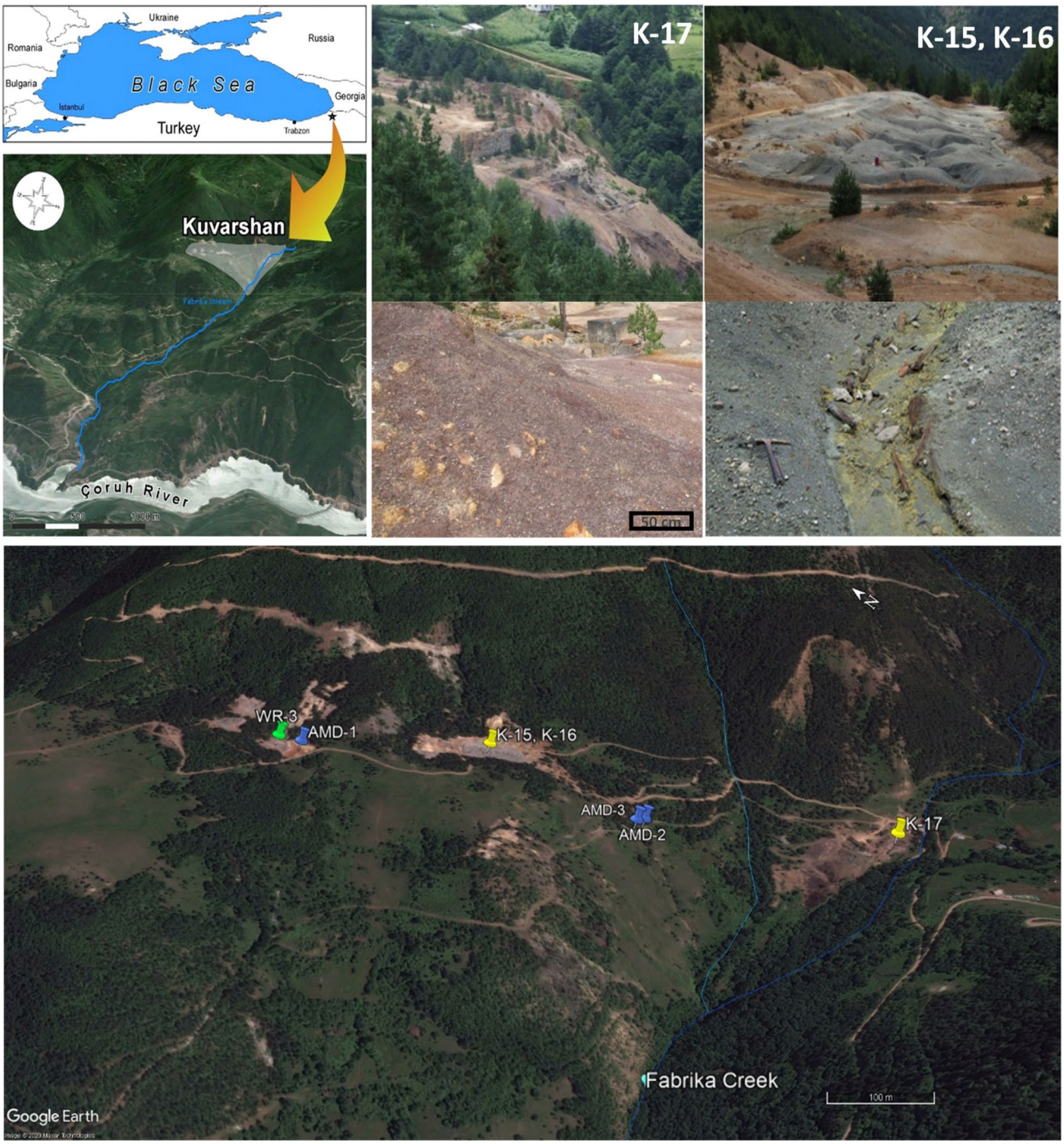

Fig. 1 Location map of abandoned Kuvarshan copper mine and sampling locations. The distribution of mine tailings (K-15, K-16, and K-17) and their close-up views are also shown. Note elemental sulfur formation on the mine tailings (K-15, K-16) and ruins of the copper smelting plant (K-17). AMD-1 and WR-3 represent acidic drainage and waste rock samples, respectively. AMD-2 and AMD-3 represent mine leachate samples. Precipitates of AMD (AMD-1p, AMD-2p, AMD-3p) were taken from the same locations where water samples were collected

40 mA and 40 kV current and voltage, Cu Kα radiation, unfiltered, 2° 2Θ/min step speed, 0°–72° 2Θ range, using a dedicated Lynxeye brand detector. The x-ray data were processed using the "PDF-2" database with the help of the "Jade 6.5" data evaluation program (MDI, California-USA). X-ray powder diffraction and semi-quantitative chemical analysis by scanning electron microscopy-energy dispersive spectroscopy (SEM–EDS) were used iteratively to identify

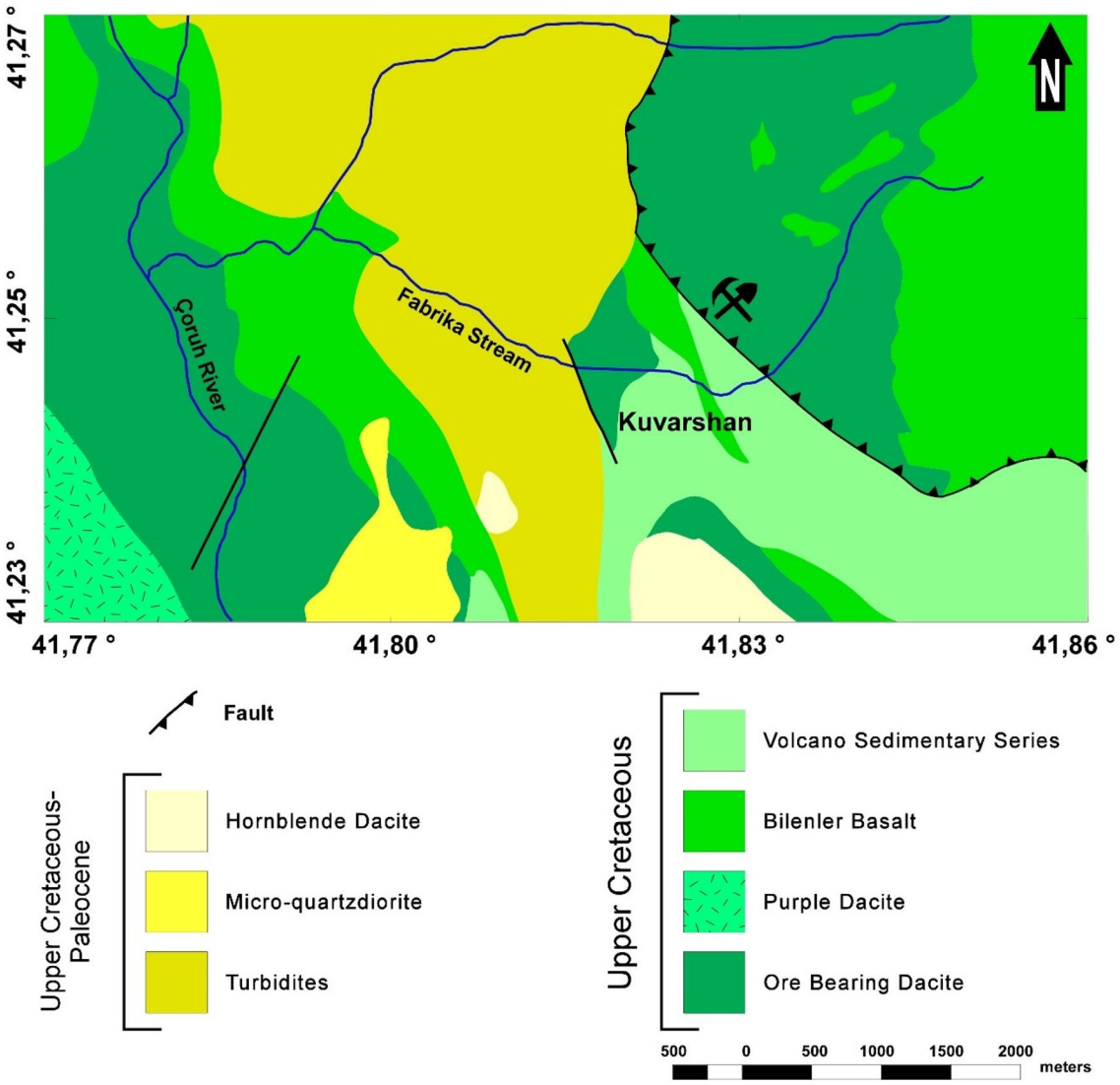

Fig. 2 Geological map of the Kuvarshan copper mine site (Taken after Van 1990)

secondary metal sulfate salts associated with AMD due to the low quantity of the mineral phases in the samples.

The kinetics of metal release and drainage chemistry resulting from the tailings were determined using a humidity cell test (ASTM D5744-07) that lasted for a year (ASTM 2001). For the humidity cell experiment (HCE; Fig. 3), ≈ 1 kg of an air-dried tailings sample with a particle size less than 6.5 mm was put in a plexiglass cell (10 cm long and 9.5 cm in diameter) and then subjected to weekly alternating cycles of three days each of dry and moist air. On the seventh day, the sample was soaked with ultrapure water (500 mL) for 2 h. The leachate was collected weekly and analyzed for several parameters, including pH, EC, oxidation–reduction potential (ORP), sulfate, and metals contents after filtering using single-use cellulose acetate syringe filters of 0.45 µm. Following the completion of the HCEs, the tailings sample in each cell was sliced into three sections (i.e. top, middle, bottom, and mixture) and analyzed via XRD for the determination of secondary mineral phases possibly formed during the experiment.

To determine the kinetics of metal release from the samples subjected to HCEs, following weekly dry/humid air cycles, the mass of metals in the leachates was calculated in mg or µg by multiplying the metal concentrations measured in the leachates with the weight of leachate collected. Then, the cumulative distribution graphs of the metal masses released over time were drawn, and the equation of the regression line and the R-squared value were determined by applying regression analysis between the time periods where the change in metal release rate occurred on the graphs. The slope of the line represents

Fig. 3 Setup of the humidity cell test

the average release rate of metals in the relevant time period (i.e. the amount of metal released from 1 kg of material per week).

Elemental analysis of the leachate samples was measured using ICP-MS (Perkin Elmer Elan DRC-e). An internal standard mix (20 ppb Re and Rh) was added to each sample online to eliminate the analytical errors resulting from the sample matrix. The pH, EC, and ORP values of the leachates were measured by a multi-parameter meter (Thermo Orion Five Star) immediately after sampling. The total acidity and alkalinity of the leachates were analyzed by titration using 1 N NaOH and 0.16 N H_2SO_4, respectively (AWWA 1995). Major anion concentrations of the samples were measured using ion chromatography (Dionex IC-1100).

The total sulfur contents of the samples were measured by a Leco carbon and sulfur analyzer (Leco SC-144DR). COM-CAT accelerator (1 g) was added to the sample (0.1 g) for complete combustion. The sulfide–sulfur content of the samples was calculated after subtracting total sulfur from the sulfate–sulfur content. To determine the sulfate–sulfur content, a mixture containing 20 mL of 3 N HCl and 5 g of the pulverized sample in a beaker was boiled and then allowed to cool down to room temperature. The final eluent was transferred to a pre-weighed PE vial, diluted with ultrapure water, and kept overnight to settle the suspended particles. The sulfate content of the eluent was then analyzed by ion chromatography.

Mineral saturation index calculations and Eh–pH mineral stability diagram of the elution were done using Geochemistry Work Bench (GWB) software (Bethke 1998). The thermodynamic dataset of thermo.tdat was used in the GWB computations.

XRF measurements were calibrated using geo-standards. The results were in good or excellent agreement with the recommended values, with a precision of $\pm 0.047\%$ (for major elements). The analyzer is precise to within less than 0.5%. The percent error for measurements lay between 0.7 and 12% for ICP-MS, 4.3–6.9% for ion chromatography, and $\approx 5.6\%$ for the LECO S analyses.

Results

Chemical and Mineralogical Characterization

Mine Tailings

Tailings cover a large area of the mine site and are very prone to both surficial erosion and oxidation processes (Fig. 1). The grain size of the tailings mainly ranges from sand to gravel size and pyrite grains are easily visible. Hematitization, kaolinization, and silicification were observed on the tailings. Traces of pyrite oxidation were also seen in dug holes on the tailings piles, indicating that the oxidation process penetrates the depths of the tailings owing to their permeability. Natural sulfur formation was also seen on the local drainages over the tailings material (Fig. 1). The mine site is located on steep slopes so surface runoff from the tailings and mine leachates drain into the local stream, which flows into the Çoruh River. AMD formation was also observed in the depressed areas of waste rock.

The tailings had a high sulfur content, ranging from 3.15 to 29%. Speciation analysis of sulfur in the tailings samples showed that the sulfide-sulfur content (0.6–26.4%)

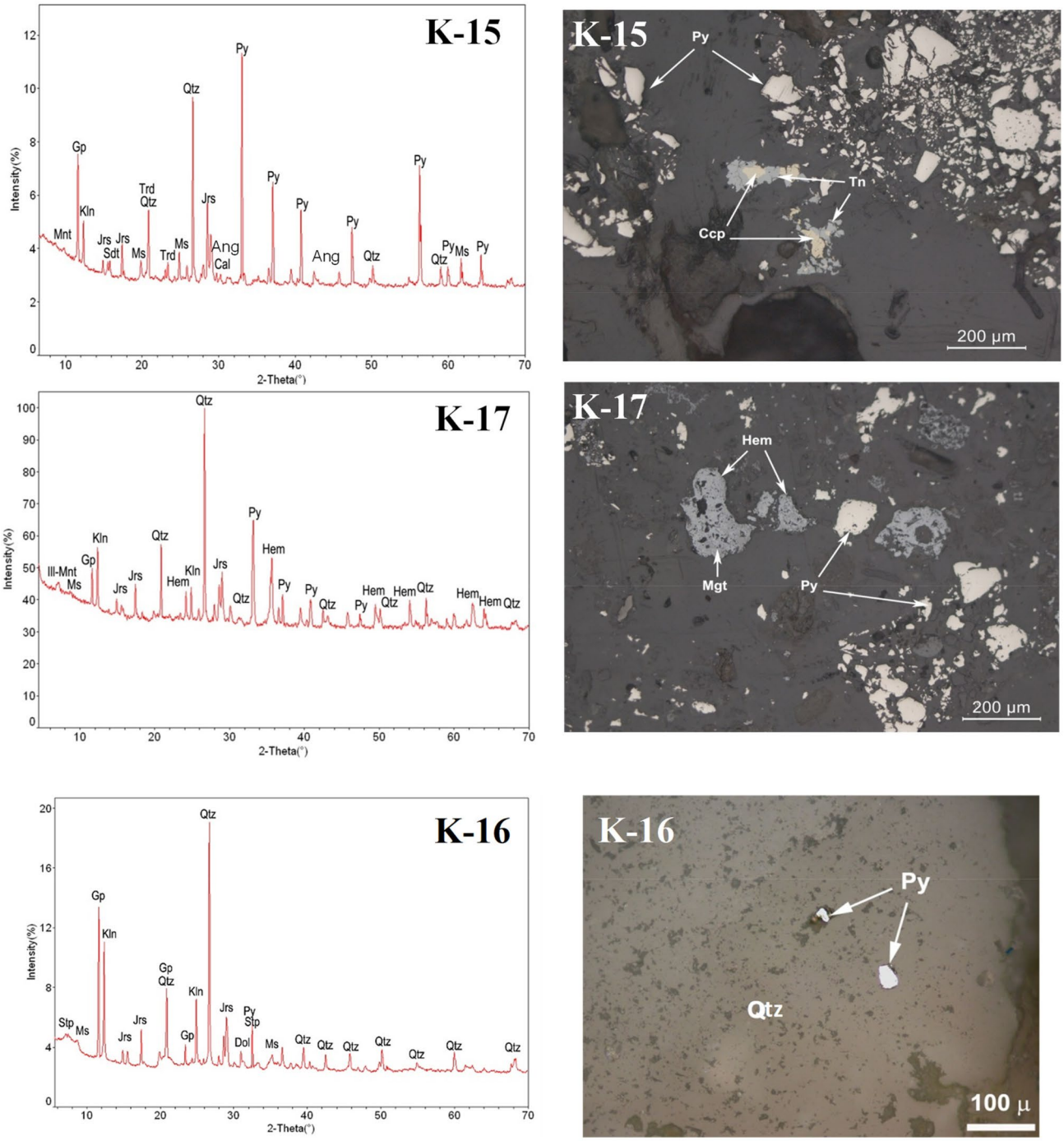

Fig. 4 XRD and polished section images of mine tailings samples. *Py* pyrite, *Ccp* chalcopyrite, *Hem* hematite, *Mgt* magnetite, *Tn* tennantite, *qtz* quartz, *gp* gypsum, *jrs* jarosite, *kln* kaolinite, *mnt* montmorillonite, *ms* muscovite, *cal* calcite, *Trd* tridymite, *Sdt* siderotil, *Ang* anglesite, *Dol* dolomite, *Stp* stilpnomelane

was the major form of sulfur, with sulfate-sulfur ranging from 1.9 to 2.9%.

The tailings were fairly rich in iron (9.4–22.2% Fe). The aluminum content of the samples ranged between 2.8 and 8.5% Al (Fig. 4). The tailings also contained substantial amounts of Cu (1787–4508 ppm), Pb (1678–4441 ppm), As (2651–6196 ppm), and Zn (440–2949 ppm) (Table 1).

Semi-qualitative analysis of the XRD measurements (Fig. 4) showed that tailings included mainly gypsum (11–25%), jarosite (8–11%), kaolinite (8–20%), illite-montmorillonite (6–9%), quartz (%15–22), and trace amounts of

Table 1 XRF analysis results of mine tailings, waste rocks, and AMD precipitates

Sample ID	Mine tailing			Waste rock	AMD precipitates-August-2011		
	K-15	K-16	K-17	WR-3	AMD-1p	AMD-2p	AMD-3p
SiO_2	18.47	38.91	26.38	18.75	41.1	9.83	5.16
Al_2O_3	5.28	16.12	5.90	3.80	12.05	13.35	1.10
Fe_2O_3	15.41	13.46	31.76	16.41	13.91	8.52	4.69
MgO	0.23	0.54	0.28	0.10	0.68	0.94	0.23
CaO	1.70	2.26	0.94	0.07	0.17	6.35	49.54
Na_2O	0.17	0.21	0.19	0.44	0.75	0.51	0.09
K_2O	0.54	2.11	0.64	0.15	1.50	0.34	0.09
TiO_2	0.17	0.57	0.27	0.15	0.73	0.19	0.05
P_2O_5	0.11	0.1	0.11	0.02	0.11	0.04	0.01
MnO	0.003	0.01	0.01	< 0.001	0.01	0.46	< 0.001
Cr_2O_3	0.02	0.02	0.02	0.02	0.02	0.44	< 0.001
SO_3	25.23	8.51	13.86	31.44	6.36	10.02	3.33
S-Leco (%)	***29.36***	***3.15***	***10.66***	***35.26***	***2.69***	–	–
Cu	1802	1787	4508	379	637	74,400	1511
Zn	523	440	2949	211	378	98,800	5263
As	5877	2651	6196	1705	22,040	1848	711
Pb	2302	1678	4441	1395	4785	735	480
Ba	6199	3591	9704	6853	1948	781	2232
Ni	54	53	69	70	37	211	< 10
Mo	51	66	156	22	107	12	< 10
Cd	< 10	< 10	< 10	< 10	< 10	290	< 10
Ag	61	53	121	41	142	78	64
Sb	110	< 10	156	< 10	357	< 10	< 10
LOI (%)	30.54	15.84	16.15	27.38	18.64	31.05	34.29
Total	***97.87***	***98.68***	***96.51***	***98.73***	***96.03***	***82.04***	***98.58***

Oxides are given in %, while trace metals are in ppm

muscovite (5–9%), calcite (5%, K-15 only), dolomite (7%, K-16 only), siderotil (5%, K-15 only), and hematite (14%, K-17 only) and showed moderate to high levels of alteration. Ore minerals in the tailings were predominantly disseminated pyrite (5–20%), with trace amounts of chalcopyrite, chalcocite, magnetite, tennantite, and sphalerite (Fig. 5). Pyrite grains in the samples ranged from 1–2 µm to 2 mm and displayed low to high oxidation. Magnetite in the tailings samples (K-17) also exhibited hematitization. Pyrite samples in K-16 also showed a high degree of alteration. Remnants of the pyrite grains in K-16 were encapsulated by quartz (Fig. 4). Microprobe analysis of pyrites in Kuvarshan showed that they contained 0.06–0.69% arsenic (TÜBİTAK 2014).

Acidic Drainages

Acidic puddles (AMD-1) were observed in low areas at the site (Fig. 5). They were isolated from the local drainage system and usually disappeared/got smaller in the dry period due to evaporation. Puddle water was characterized by ochre color (Fig. 5). Wet and dry period sampling indicated that this puddle water was highly acidic (pH: 2.4) with an EC between 3610 and 7780 µS/cm and was Fe–SO_4 type. The DO content of the acidic water ranged between 2.7 and 3.1 mg/L. The acidic puddle water was characterized by high sulfate (2458–10,782 mg/L) and metal (Fe, Al, Cu, Zn, and Mn) contents (Table 2). Fe (176–1830 mg/L) was the highest dissolved metal in the acidic water, followed by Al (33–349 mg/L), Cu (6–80 mg/L), Zn (3.9–39 mg/L), and Mn (3.7–9.0 mg/L). Dissolved concentrations of potentially toxic metals such as arsenic, lead, and cadmium in acidic water were 359–924, 125–165, and 14.5–44.1 µg/L, respectively (Fig. 6, Table 2). The changes in the solid/water ratio due to evaporation caused the seasonal variations observed in the concentrations of chemical contents.

The distribution of metals (dissolved vs. particulate phase) in the acidic water was also determined by analyzing filtered and unfiltered water samples. Unfiltered water samples were subject to microwave digestion with nitric acid according to the EPA 3015A method before chemical analysis. Total (dissolved + suspended) concentrations of metals in acidic water are presented in Fig. 6 and Table 3. Al (86%), Mn (100%), Cu (84%), Zn (85%), and Pb (%80) were mainly

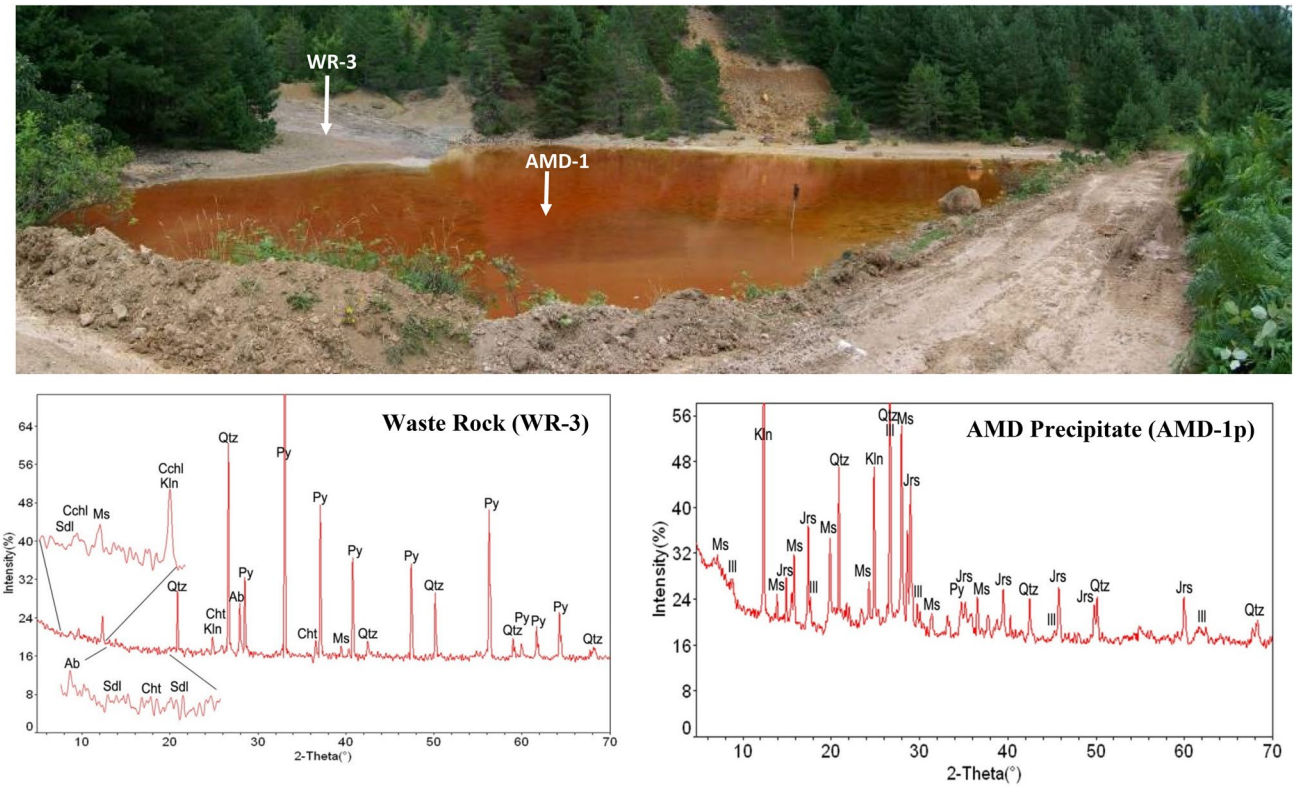

Fig. 5 Acidic puddles developed on the waste rocks and XRD images of waste rock (WR-3) and AMD precipitates (AMD-1p). *Py* pyrite, *Cht* chalcanthite, *Jrs* jarosite, *Sdl* siderotil, *Kln* kaolinite, *Ill* illite, *Qtz* quartz, *Ms* muscovite, *Cchl* clinochlore, *Ab* albite

found in the dissolved phase while a large fraction of the total Fe (73%) and As (98%) was present in the suspended phase in the acidic water (Tables 2 & 3). Jarosite was the main AMD product found in the puddle precipitate sampled for mineralogical characterization (Fig. 5). This suggests that high Fe and As concentrations in the suspended phases are likely related to jarosite. Other minerals detected in the precipitate sample were feldspar, kaolinite, illite, quartz, muscovite, and pyrite. Except for the jarosite, all of these minerals were also observed in the mine waste rock materials located around the puddle (Fig. 5). This indicated that the AMD precipitate sample was likely contaminated with mine waste as it was sampled.

Mine Leachates

Mine leachates, which were likely discharged from collapsed galleries (Fig. 7) were turquoise in color with a slightly acidic character (pH: 4.9–6.5). Their EC values ranged between 3940 and 4340 µS/cm (Table 2). Mine leachates contained high Ca (617–643 mg/L), Mg (404–410 mg/L), and SO_4 (3078–4839 mg/L) contents and were a Mg-Ca-SO_4 type. In addition, they contained high metal loads, which showed significant seasonal variability in concentration. Metals having high total concentrations were Al (42–158 mg/L), Cu (45–111 mg/L), Zn (72–79 mg/L), Mn (23–29 mg/L), and Fe (6.1–26 mg/L) (Table 3) along with elevated Co (350–812 µg/L), Ni (301–319 µg/L), Cd (290–390 µg/L), As (33–181 µg/L), and Pb (34–107 µg/L). Concentrations of these metals significantly exceeded the permissible quality standard values described in the national regulation of surface water quality. Analysis of filtered leachate samples showed that Al, Fe, Cu, and Pb (89–99.8% of total concentration) were found predominantly in the suspended phase in mine leachate during the dry period while the other metals such as Mn (100%), Co (96%), Ni (79%), Zn (72%), As (69%) and Cd (66%) remained in the dissolved phase. On the other hand, during the wet period most of the metals (i.e., Al, Cu, Zn, Mn, Co, As: 96–99%, Cd: 80%, Ni & Pb: 62–65%) except for Fe (33%) were found in the dissolved phase and their dissolved phase concentrations showed a significant increase compared to those in the dry period (Fig. 6, Tables 2 and 3).

Precipitates sampled in wet and dry periods were analyzed using XRD and SEM–EDS to determine the mineral phases causing significant seasonal changes in the metal loads of the mine leachates. XRD analyses of the samples identified highly soluble sulfate salts including chalcoalumite ($CuAl_4SO_4(OH)_{12}\cdot 3H_2O$), chalcocyanite ($CuSO_4$), goslarite ($ZnSO_4\cdot 7H_2O$), coquimbite ($Fe_2(SO_4)_3\cdot 9H_2O$),

Table 2 Dissolved chemical contents of acidic drainages and mine leachates in the abandoned Kuvarshan mine site

Sample ID	Units	AMD-1	AMD-1	AMD-2	AMD-2	AMD-3	AMD-3
Sampling period		August 2011	May 2012	August 2011	May 2012	August 2011	May 2012
T	°C	25.2	16.2	16.7	11.8	23.5	16.1
pH	-	2.4	2.4	6.5	4.9	8.0	8.4
DO	mg/L	3.1	2.7	5.4	7.4	5.3	6.3
EC @ 25 °C	µS/cm	3610	7780	3940	4340	2920	2635
Na^{+}	mg/L	15	< 0.2	38	69	36	71
K^{+}	mg/L	< 0.2	< 0.2	< 0.2	135	< 0.2	< 0.2
Mg^{+2}	mg/L	21	525	410	404	298	301
Ca^{+2}	mg/L	95	1549	617	643	346	439
Cl^{-}	mg/L	1.6	1.7	< 0.5	< 0.02	1.9	< 0.02
SO_4^{-2}	mg/L	2458	10,782	3078	4839	1661	1640
HCO_3^{-}	mg/L	0	0	134	0	374	423
F^{-}	mg/L	0.9	0.3	< 0.05	0.2	< 0.05	< 0.05
Fe	mg/L	176	1830	0.2	8.7	< 0.0001	0.02
Cu	mg/L	6.0	80	4.7	108	0.1	0.02
Al	mg/L	33	349	0.08	151	0.05	0.004
Zn	mg/L	3.9	39	51	78	1.1	0.32
Mn	mg/L	3.7	9.0	22.8	29.0	0.04	0.032
Co	µg/L	148	1022	337	800	2.2	1.5
Ni	µg/L	37	106	239	198	12	14
As	µg/L	924	359	23.2	176	5.7	3.7
Mo	µg/L	5.4	66.0	0.7	0.3	0.7	0.6
Ag	µg/L	1.09	0.4	0.02	< 0.01	< 0.01	< 0.01
Cd	µg/L	14.5	44.1	259	232	3.7	1.1
Pb	µg/L	165	125.0	9.5	22	0.10	< 0.01
Tl	µg/L	42.9	5.9	0.7	0.34	0.1	0.10
Hg	µg/L	< 0.01	0.04	< 0.01	< 0.01	< 0.01	< 0.01
Ba	µg/L	6.61	5.5	7.3	0.4	3.1	2.8
Sb	µg/L	–	28.7	–	0.2	–	0.4
Water type		Fe–SO_4	Fe–SO_4	Mg–Ca–SO_4	Mg–Ca–SO_4	Mg–Ca–SO_4	Mg–Ca–SO_4
X		41° 49′ 0.07″ E	41° 49′ 0.07″ E	41° 49′ 10.46″ E	41° 49′ 10.46″ E	41° 49' 9.98″ E	41° 49' 9.98″ E
Y		41° 15' 5.43″ N	41° 15' 5.43″ N	41° 14′ 51.51″ N	41° 14′ 51.51″ N	41° 14′ 51.72″ N	41° 14′ 51.72″ N

rozenite ($FeSO_4 \cdot 4H_2O$), and gypsum ($CaSO_4 \cdot 2H_2O$) in precipitates (Fig. 7). Bulk chemical analysis of the precipitate (AMD-2p, Table 1) indicated that the turquoise colored precipitates were rich in Zn (9.9%), Cu (7.4%), Al (7.1%), and Fe (6.0%) and also contained a considerable amount of As (1848 ppm), Pb (735 ppm), Cd (290 ppm), and Ni (211 ppm). The SEM–EDS studies also showed that efflorescence sulfate salts were present in the precipitates and weakly crystalline in habit. The SEM–EDS spectra of individual secondary sulfate phases indicated that miscellaneous assemblages with Cu, Fe, Ca, and Al-sulfates had precipitated from the leachates and showed seasonal variations in amount and type (Fig. 8).

Efflorescent sulfate salts are commonly observed in abandoned copper mines and were observed locally in a limited area of the mine site (Figs. 1 and 7). These mineral phases form as a sequence of reactions including oxidation, hydrolysis, and evaporation, and are affected easily by seasonal conditions (Hammarstrom et al. 2005). They have high metal loads and can dissolve rapidly in wet seasons, hence causing high metal concentrations in mine leachates (Carbone et al. 2013; Hammarstrom et al. 2005). Analysis of both mine leachates and precipitates indicated that the formation of sulfate salts in the Kuvarshan copper mine governed the recycling of Cu, Al, and Fe in the mine discharges. Dissolution of highly soluble metal sulfate precipitates greatly increased

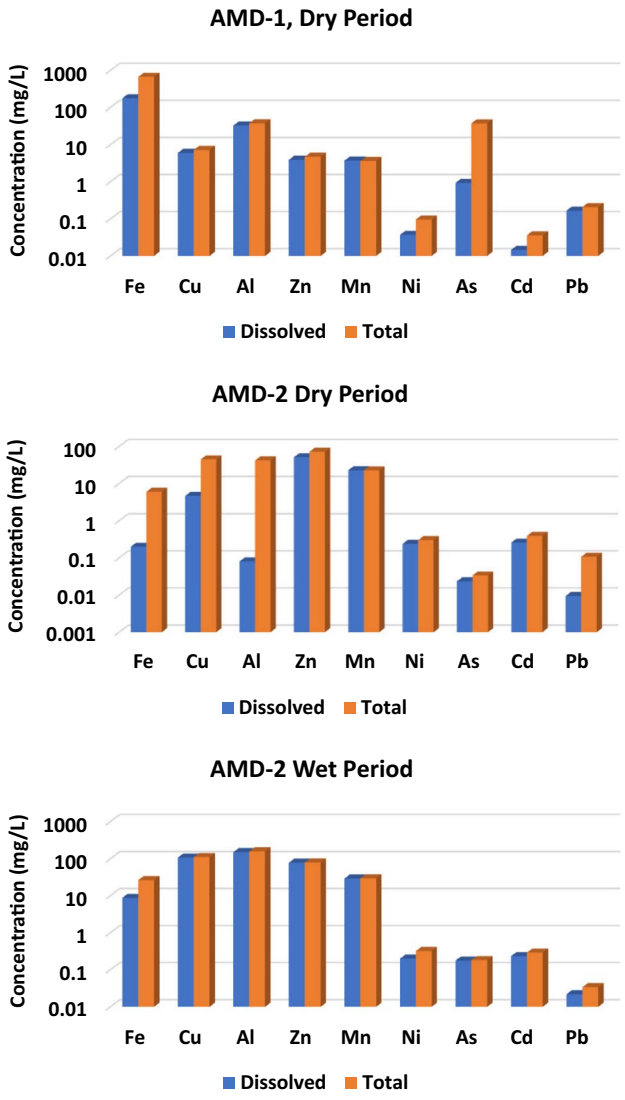

Fig. 6 Variation observed in dissolved and total metal concentrations of acidic drainages (AMD-1) and mine leachates (AMD-2)

the elution concentrations of Al, Cu, Fe, Zn, and As in the wet season, releasing high metal loads to the nearby stream (Figs. 1 and 9).

Alkaline seepages (pH: 8.0–8.4) were also observed in a limited area of the mine site and caused the deposition of aragonite in encrusting forms about 10 m north of the turquoise mine drainage (Fig. 10). Their EC values ranged between 2635 and 2920 µS/cm and were rich in Ca (346–439 mg/L), Mg (298–301 mg/L), SO_4 (1640–1661 mg/L), and HCO_3 (374–423 mg/L), but with low metal contents (Zn: 0.7 mg/L, Fe: < 1 µg/L, Cu:30 µg/L, Ni: 22 µg/L, Al: 50 µg/L, As: 5.4 µg/L, Cd:0.8 µg/L, Pb: 0.04 µg/L) (Table 2). On the other hand, bulk chemical analysis of the aragonite deposit showed enrichment in metal content (Zn: 5263 ppm, Cu: 1511 ppm, As: 711 ppm, and Pb: 480 ppm, Table 1). These results suggested that zinc, copper, arsenic, and lead metal ions had coprecipitated with aragonite and been removed from the alkaline seepage water. The alkaline seepages in the mine site may be due to contact of infiltrating rainwater with carbonate strata in the volcanic-sedimentary units overlaying the ore-bearing dacite. The precipitation of aragonite instead of calcite in an abandoned copper mine can be due to several factors, including the local geochemical conditions (pH, temperature, pCO_2) and the presence of trace elements such as Mg and Sr. Aragonite tends to precipitate at higher temperatures and CO_2 levels, and lower pH values than calcite (Zeller and Wray 1956). The presence of magnesium and strontium ions can also promote the formation of aragonite (De Choudens-Sanchez and Gonzales 2009; Sunagawa et al. 2007). The temperature of the water is also low, ≈ 16 °C. We postulate that a high concentration of Mg in water promotes aragonite precipitation over calcite at this site (De Choudens-Sanchez and Gonzales 2009).

Table 3 Total metal concentrations of unfiltered acidic drainages (AMD-1T) and mine leachates (AMD-2T) in abandoned Kuvarshan mine site

Sample ID	Units	AMD-1T	AMD-2T	AMD-2T
Sampling period		August 2011	August 2011	May 2012
Fe	mg/L	666	6.06	26.3
Cu	mg/L	7.2	44.7	111
Al	mg/L	38.0	42	158
Zn	mg/L	4.7	71.6	79
Mn	mg/L	3.6	22.7	29.4
Co	µg/L	260	350	812
Ni	µg/L	96.3	301	319
As	µg/L	37,643	33.4	181
Mo	µg/L	45.4	4.1	0.2
Ag	µg/L	2.8	0.25	0.02
Cd	µg/L	36.2	390	290
Pb	µg/L	205.3	107	34
Tl	µg/L	51.8	0.9	0.35
Hg	µg/L	2.0	1.4	< 0.01
Ba	µg/L	24.3	25.0	< 0.1
Sb	µg/L	–	–	0.2

Total concentration represents the sum of dissolved and suspended phase metal concentrations in the sample solution

Metal Release Rates and Mechanisms

The HCEs were run on mine wastes (K-15, K-17, Table 1) for a 1-year duration to determine drainage chemistry and the release rate of chemical constituents. The ORP of eluates ranged between 263 and 601 mV during the test, indicating that oxidizing conditions prevailed in the cells. The water facies of the eluates monitored during the HCEs

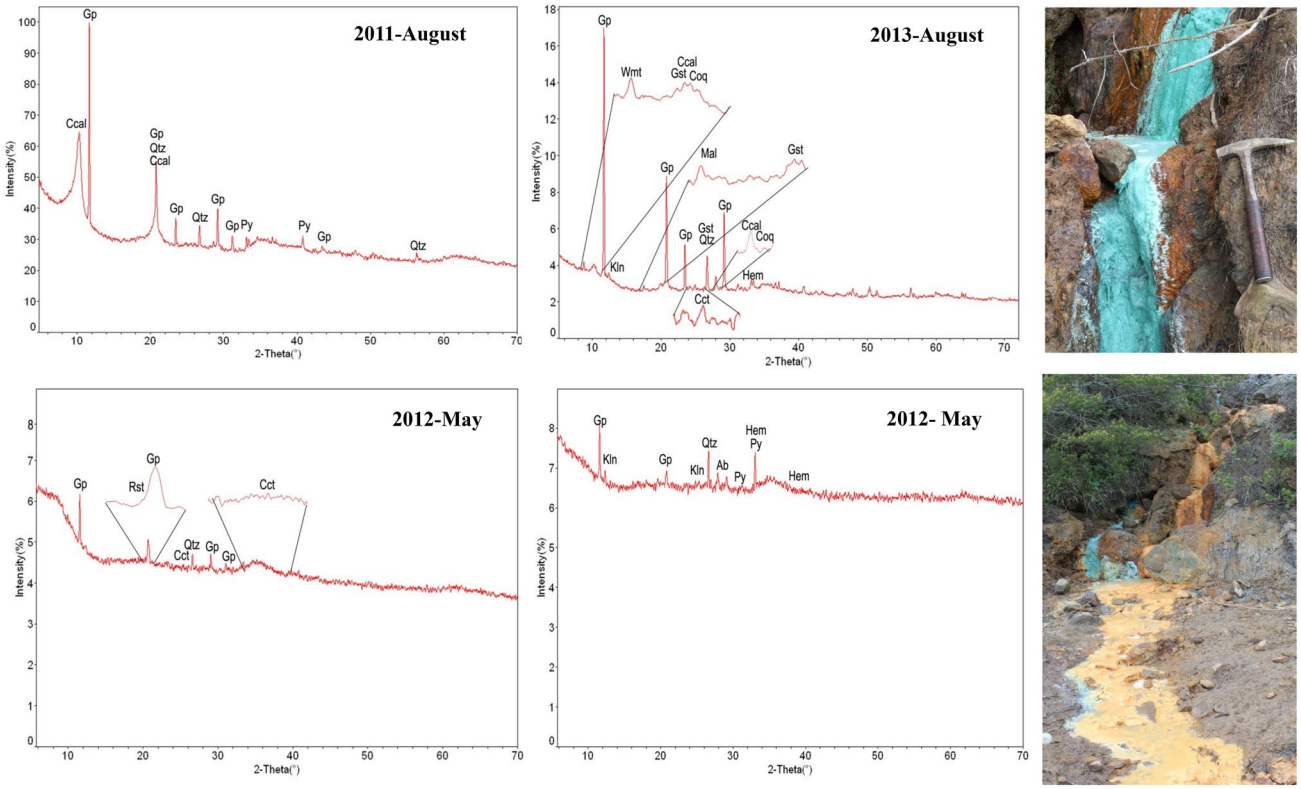

Fig. 7 XRD images of mine leachate precipitates (AMD-2p) at wet and dry periods. Photos of mine leachates (AMD-2) are shown on the right of XRD images. *Py* pyrite, *Ccal* chalcoalumite, *Cct* chalcocyanite, *Rst* rozenite, *Coq* coquimbite, *Gst* goslarite, *Gp* Gypsum, *Mal* malachite, *Wmt* whitmoreite (?/possible), *Hem* hematite, *Kln* kaolinite, *Qtz* quartz; *Ab* albite

also changed, initially from Fe–SO_4 to $CaSO_4$, and later to Fe–SO_4 and H–SO_4 water types.

Leachates obtained from the tailings showed a strongly acidic character with a pH value ranging from 1.4 to 2.8 throughout the tests (Fig. 11). The eluate pH showed a rise for the first 5 to 11 weeks (i.e. depending on the waste material), then exhibited a descending trend, and eventually stabilized. Sulfate concentrations ranged between an average 3.1 ± 2.0 g/L and 3.5 ± 1.4 g/L (Fig. 11) following the first-week rinse. The rate of sulfate release was initially (< 2 weeks) fast (10–15 g kg^{-1} rock $week^{-1}$), then slowed down to 0.9–1.2 g kg^{-1} rock $week^{-1}$ before increasing to (1.2–1.6 g kg^{-1} rock $week^{-1}$; Figs. 12 & 13).

The initially fast rates of metal release were from easily exchangeable sites on the mineral surfaces. The later decrease in the rate of metal release was controlled by the rate-limited desorption process or dissolution kinetics of the mineral phases. During the HCEs, a decrease in the rate of metal release was followed by a later increase. The increase in the rate of sulfate and iron release, along with a decrease in leachate pH, indicated the initiation of pyrite oxidation in the tailings samples (Figs. 12 and 13). An increase in As and Zn release rates also coincided with the initiation of pyrite oxidation, suggesting a common origin. The eluate SO_4/Fe molar ratio approached 2 towards the later periods of the experiments (Fig. 14), suggesting that pyrite oxidation dominated Fe and SO_4 release. After the initiation of pyrite oxidation, while the mean pH value of the elution was ≈ 2, sulfate and metals in the leachate ranged between 3627 and 3992 mg/L for SO_4, 848–988 mg/L for Fe, 3.4–8.7 mg/L for As, and 1.4–4.0 mg/L for Zn, respectively (Fig. 11).

Geochemical modeling of the eluates in the HCEs showed that $FeSO_4^+$ is the dominant Fe species in the eluent with weekly samples, slightly outside the jarosite-K field on the Eh–pH diagram (supplemental Fig. S-1). Calculations of mineral saturation indices of the eluates also revealed that the eluents remained undersaturated with respect to jarosite and gypsum during the experiment (supplemental Fig. S-2). The results indicated that jarosite dissolution also contributed to Fe and SO_4 enrichment in the HCE leachates.

Metal release rates from different samples (K-15/K-17) were evaluated considering whole-rock chemical compositions as well (Table 1, Figs. 12 and 13). The initial release rates occurred at a greater rate for samples (K-17) having high metal content. However, in the later time periods of the HCEs, the release rates of most metals resembled each other or were of the same order of magnitude. For instance, Fe release rates for K-15 and K-17 were 346 and 362 mg/

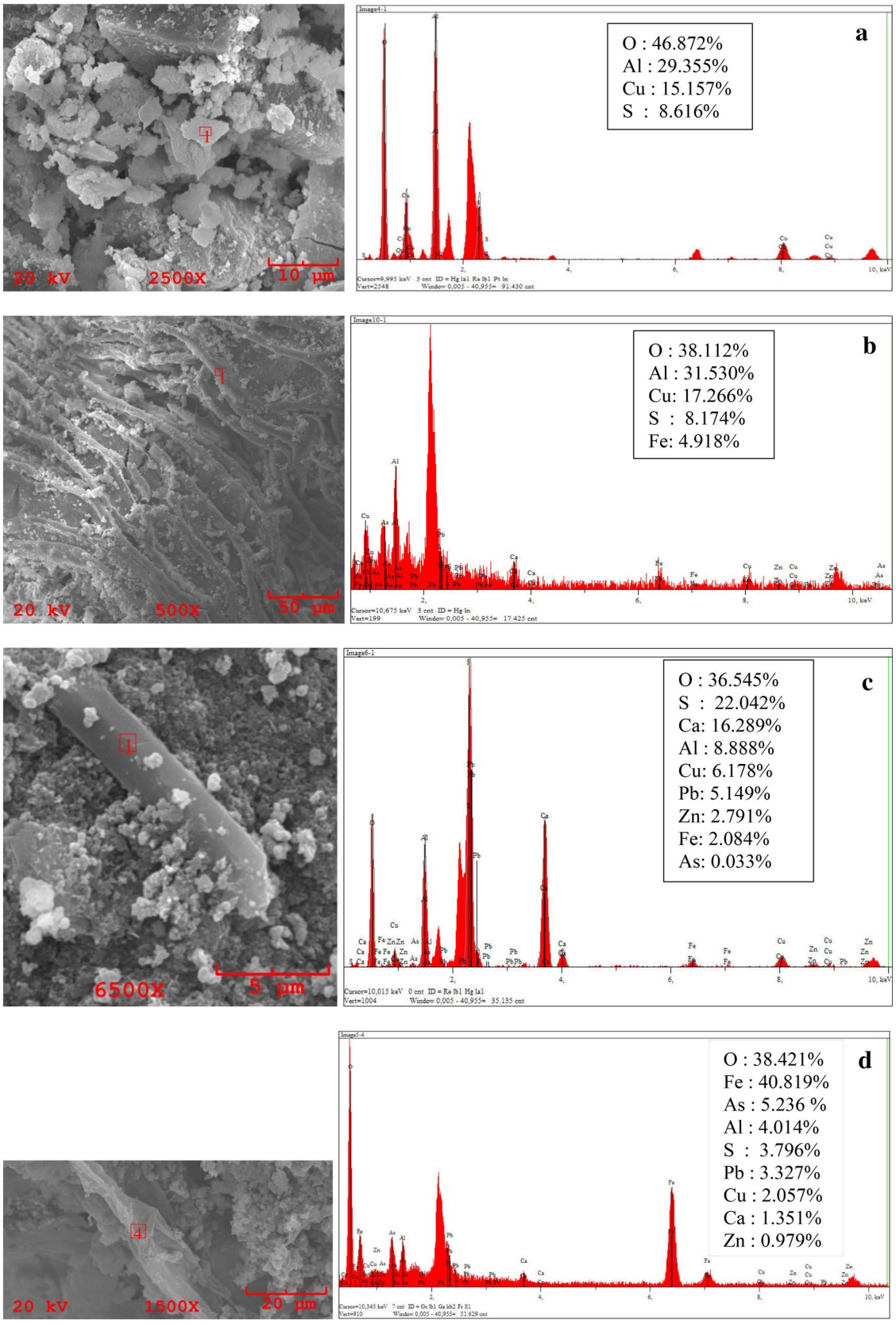

Fig. 8 SEM–EDX images of secondary minerals obtained from mine leachate precipitates (AMD-2p). **a** Chalcoalumite, **b** iron-rich chalcoalumite, **c** hydrous calcium aluminum sulfate mineral (?), **d** Al-substituted ferrihydrite

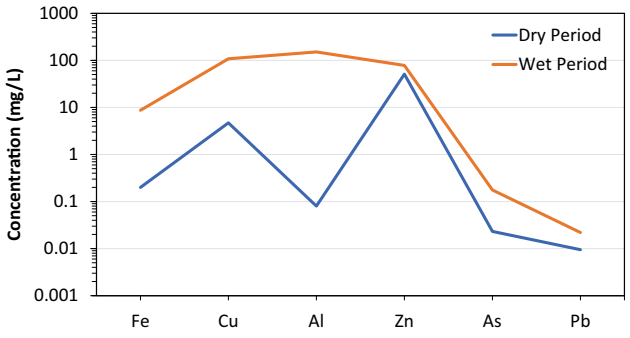

Fig. 9 Seasonal variation observed in dissolved metal concentrations of mine leachates (AMD-2)

kg rock/week, respectively. This indicated that pyrite oxidation mainly controlled Fe release in the later periods of the HCEs. SO_4, Cu, Zn, As, and Al release rates for K-15 and K-17 samples at the later time periods also took place in similar order magnitudes (1601–1237, 1.2–1.7, 0.6–0.5/1.4, 1.3–2.9, and 2.2–2.4/5 mg/kg rock/week, respectively). On the other hand, a significant difference was observed in Pb release rates observed in the K-15 and K-17 samples. A greater and constant Pb release rate was attained in K-15 (0.9 mg/kg rock/week), which contained anglesite, although the Pb concentration in K-17 (0.02–0.05 mg/kg rock/week) was almost double that of K-15 (Table 1).

The tailings samples subjected to HCEs were analyzed via XRD at the end of the experiment to determine the secondary mineral phases formed during oxidation of the sulfide minerals (mainly pyrite). Changes in the pre- and post-HCE mineral abundances/phases of the pre-and post-HCE tailings were compared (Table S-1, Fig. S-3). Semi-quantitative analyses of the mineral phases revealed that the abundance of gypsum dropped in both samples. A similar drop was also seen in the abundance of pyrite, but only in the K-15 sample. There were only small changes in the abundance of the other primary mineral phases (Table S-1, Fig. S-3). Mineral saturation indices of eluates from K-15 showed undersaturation with respect to jarosite but occasional oversaturation for K-17 during the HCEs. This indicated that jarosite precipitation conditions developed in K-17 during HCE. XRD analyses also showed that hydrated iron sulfate minerals (6–9%), such as copiapite and meta-hohmanite, had precipitated based on the difference from the initial mineral content of the tailings during the experiment

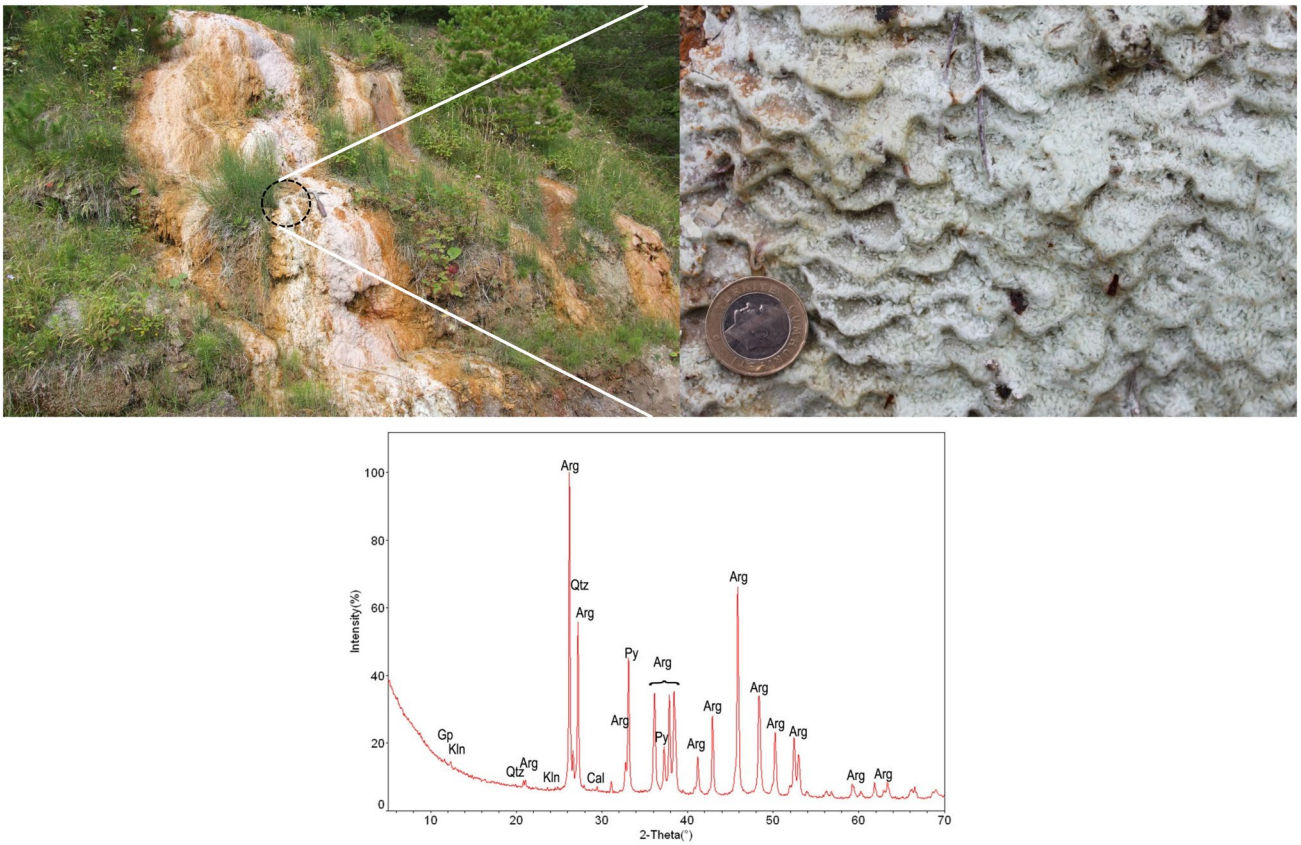

Fig. 10 XRD image of Aragonite precipitate (AMD-3p) formed from alkaline mine drainages. *Arg* aragonite, *Py* pyrite, *Cal* calcite; *Kln* kaolinite; *Qtz* quartz, *Gp* gypsum

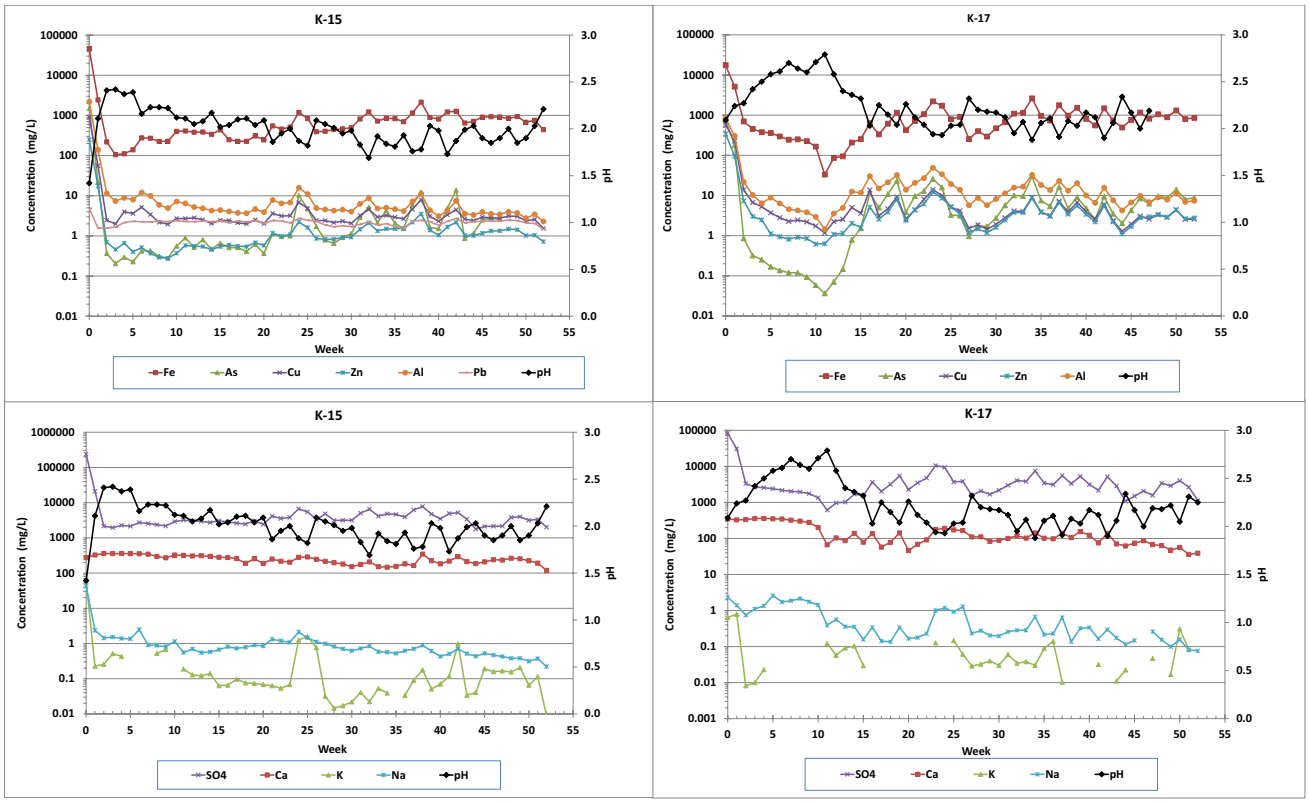

Fig. 11 Elution behavior of metals from mine tailings samples (K-15, K-17) during HCEs

(Fig. S-4). These results provide evidence of both gypsum dissolution and pyrite oxidation.

Within the context of the study, the chemical compositions of eluates obtained from the HCEs were also compared to the acidic drainage (AMD-1) that formed in the tailings (Table 2). The results showed that the pH and ECs of the eluates resembled AMD-1 and were 2.1 and 5562 µS/cm, respectively. The dominant water type observed in the eluate (Fe–SO_4) also exhibited similarity to that of AMD-1 (Table 2). The average metal contents of the eluate also showed resemblances to AMD-1 (Table 2). Concentrations of the metals in decreasing order were as follows: Fe (688 mg/L) > Al (9.6 mg/L) > As (4.3 mg/L) > Cu (3.7 mg/L) > Zn (2.2 mg/L). Eluates also had a rich metal content similar to that of AMD-1. The HCEs showed that the tailings produced similar eluate chemistry to the AMD observed at the mine site.

The elution behavior of metals, the changes in mineral abundances/phases of tailings samples, mineral contents of the tailings, and geochemical modeling results of eluates from HCEs suggested that the following reactions were controlling the elution chemistry and mineral phases formed during the tailings oxidation. Most of these reactions are commonly seen in sulfidic tailings around the world (Dold 2014; Jambor et al. 2000; Nordstrom and Alpers 1999).

Oxidation of sulfide minerals in mine tailings is described by:

$$FeS_{2(Pyrite)} + 3.5\,O_2 + H_2O \rightarrow Fe^{2+} + 2\,SO_4^{2-} + 2H^+$$

$$Fe^{2+} + 0.25\,O_2 + H^+ \rightleftharpoons Fe^{3+} + 0.5\,H_2O (pH < 3.5)$$

$$Fe^{3+} + 2\,H_2O \rightleftharpoons FeOOH_{(S)\,(Ferrihydrite)} + 3\,H^+$$

$$FeCuS_{2(Chalcopyrite)} + 4\,O_2 \rightarrow Fe^{2+} + Cu^{2+} + 2\,SO_4^{2-}$$

$$ZnS_{(Sphalerite)} + 2\,O_2 \rightarrow Zn^{2+} + SO_4^{2-}$$

Mineral dissolution reactions during AMD formation include:

$$(Na,\ K)Fe_3(SO_4)_2(OH)_{6(Jarosite)} + 6H^+ \rightarrow (Na^+ \text{or } K^+) + 3\,Fe^{3+} + 2\,SO_4^{2-} + 6\,H_2O\,(pH < 3.5)\,(K-15\ \text{only})$$

$$CaSO_4 \cdot 2\,H_2O_{(gypsum)} \rightleftharpoons Ca^{2+} + SO_4^{2-} + 2\,H_2O$$

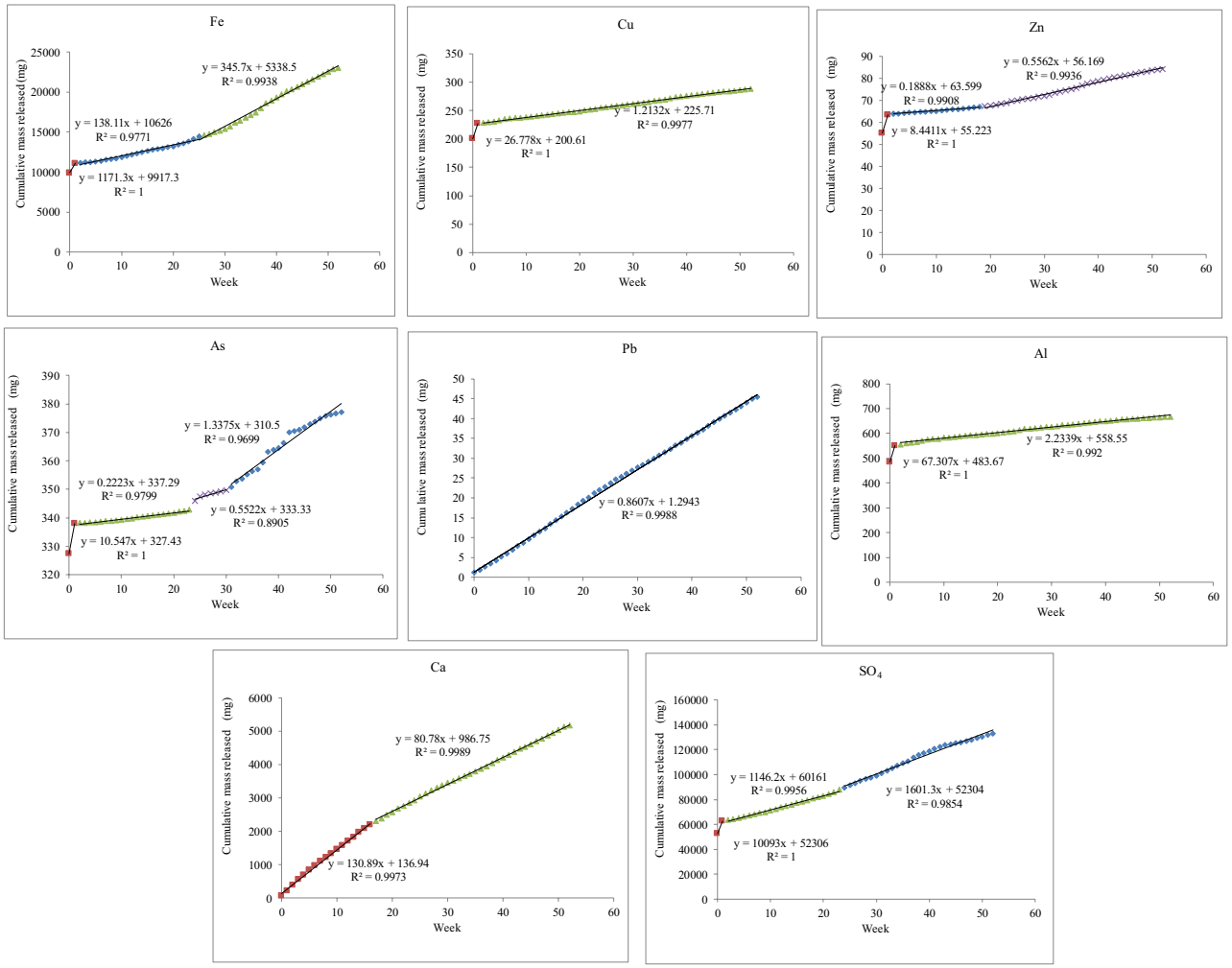

Fig. 12 Change in metal release rate obtained from mine tailings sample (K-15) during humidity cell test. The slope of the lines represents the metal release rate in each time period

$$K_{0.01}Na_{0.56}\left(Al_{3.13}Mg_{0.45}Fe^{3+}_{0.32}Fe^{2+}_{0.06}Ti_{0.01}\right)\left[Si_{7.98}Al_{0.02}\right]O_{20}(OH)_{4(\text{Kaolinite})} + 12.08\,H^{+} + 7.92\,H_2O \rightarrow 0.01K^{+} + 0.56\,Na^{+} + 3.15\,Al^{3+} + 0.32\,Fe^{3+} + 0.06\,Fe^{2+} + 0.45\,Mg^{2+} + 0.01\,Ti^{4+} + 7.98\,H_4SiO_4$$

$$S^{0}_{(\text{Native sulfur})} + H_2O + 3/2\,O_2 \rightarrow 2\,H^{+} + SO^{2-}_{4}(\text{at the initial time periods of HCE})$$

$$CaCO_{3(s)\,(\text{Calcite})} + H^{+} \rightleftharpoons Ca^{2+} + HCO^{-}_{3}(K-15\ \text{only})$$

$$PbSO_{4(\text{Anglesite})} \rightleftharpoons Pb^{2+} + SO^{2-}_{4}(K-15\ \text{only})$$

Mineral precipitation reactions during AMD formation include:

$$\left(Na^{+}\text{or}\,K^{+}\right) + 3\,Fe^{3+} + 2\,SO^{2-}_{4} + 6\,H_2O \rightarrow (Na,\ K)Fe_3\left(SO_4\right)_2(OH)_{6(\text{Jarosite})} + 6\,H^{+}(K-17\ \text{only})$$

$$Fe_2\left(SO_4\right)_2(OH)_2 \cdot 3\,H_2O_{(\text{Metahohmanite})}\text{and}\,Fe_{14}O_3\left(SO_4\right)_{18} \cdot 63\,H_2O_{(\text{Copiapite})}\text{precipitation.}$$

Conclusion

This study revealed the geochemical processes and mineral phases that control the contents of mine leachate and the rates of metal release from tailings in an abandoned copper mine. The results of detailed geochemical and mineralogical characterization of the tailings and leachates showed that

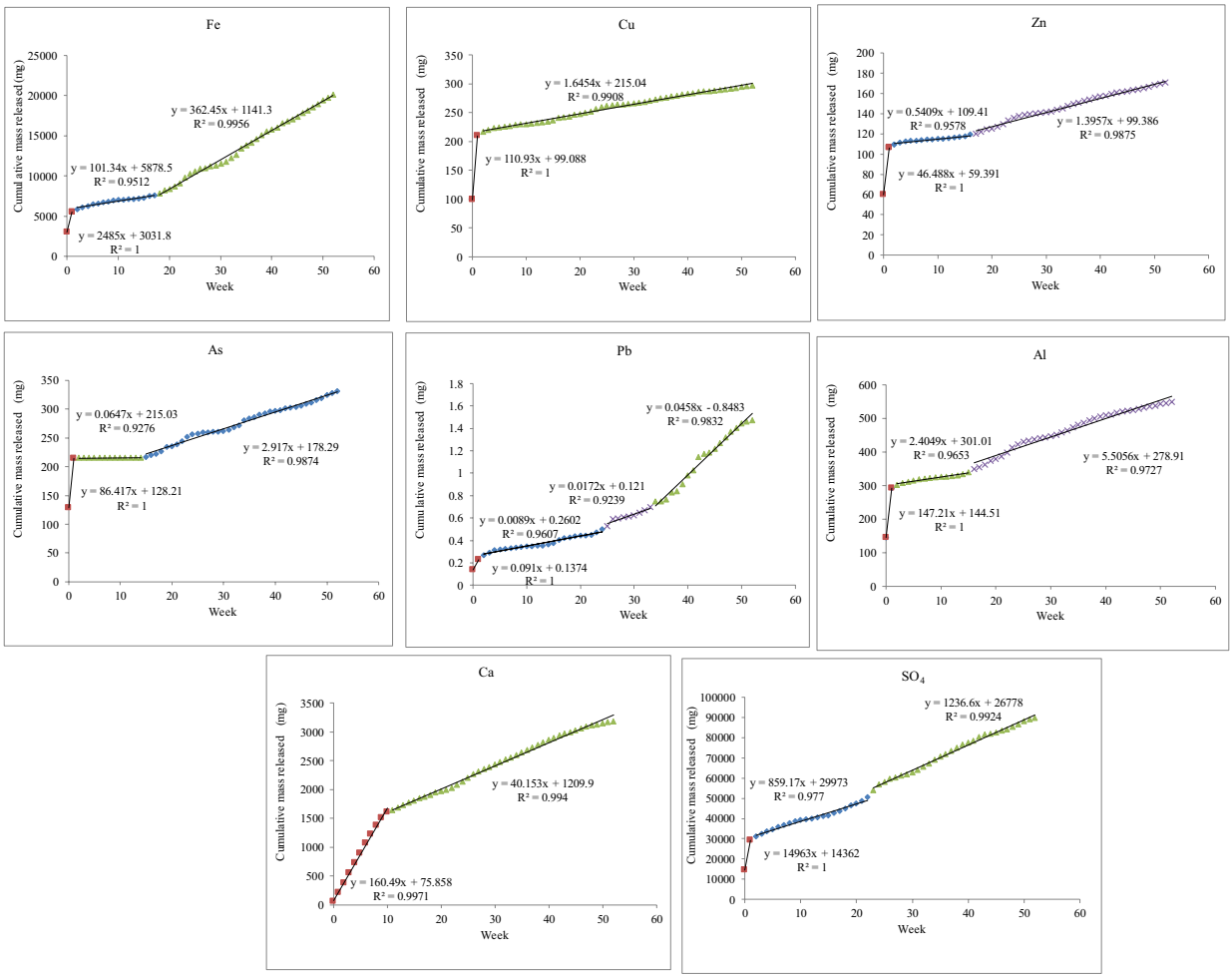

Fig. 13 Change in metal release rate obtained from mine tailings sample (K-17) during humidity cell test. The slope of the lines represents the rate of metal release in each time period

the oxidation of pyrite in the tailings was responsible for the formation of acidic drainages (pH ≈ 2.7–3.1) with high sulfate and metal contents (Fe > Al > Cu > Zn > Mn > As > Pb > Cd). Jarosite precipitate that formed in the acidic and sulfate-rich environment as a result of pyrite oxidation controlled the sequestration of Fe and As in the AMD. XRD and SEM–EDX studies indicated that highly soluble metal sulfate salts, including chalcoalumite, chalcocyanite, goslarite, coquimbite, and rozenite, also precipitated locally in the mine site from mine leachates. The dissolution of these highly soluble metal sulfate precipitates during the wet season significantly increased the concentrations of Al, Cu, Fe, Zn, As, and Pb in the mine leachates, and hence the metal loads to a nearby stream. On the other hand, the precipitation of aragonite from alkaline mine leachates at the mine site removed Zn, Cu, As, and Pb metal ions from the solution and minimized the release of these metals into the environment. Geochemical modeling of the HCEs revealed that $FeSO_4^+$ was the dominant Fe species in the acidic eluents. The dissolution of jarosite and gypsum also contributed to the enrichment of Fe and SO_4. An increase in As and Zn release rates coincided well with the initiation of pyrite oxidation during the HCEs, pointing to a common origin of their release. In conclusion, improper disposal of tailings in abandoned sulfide mine sites leads to soil and water pollution and creates a significant environmental risk for surrounding ecosystems. This study demonstrates that precipitation or dissolution of secondary hydrated sulfate minerals from mine leachates can act as a seasonal sink or source for various metals and govern the distribution of potentially toxic metals between aqueous and solid phases. Therefore, proper management of secondary sulfate minerals is a crucial aspect to consider when addressing environmental remediation efforts at abandoned copper mines.

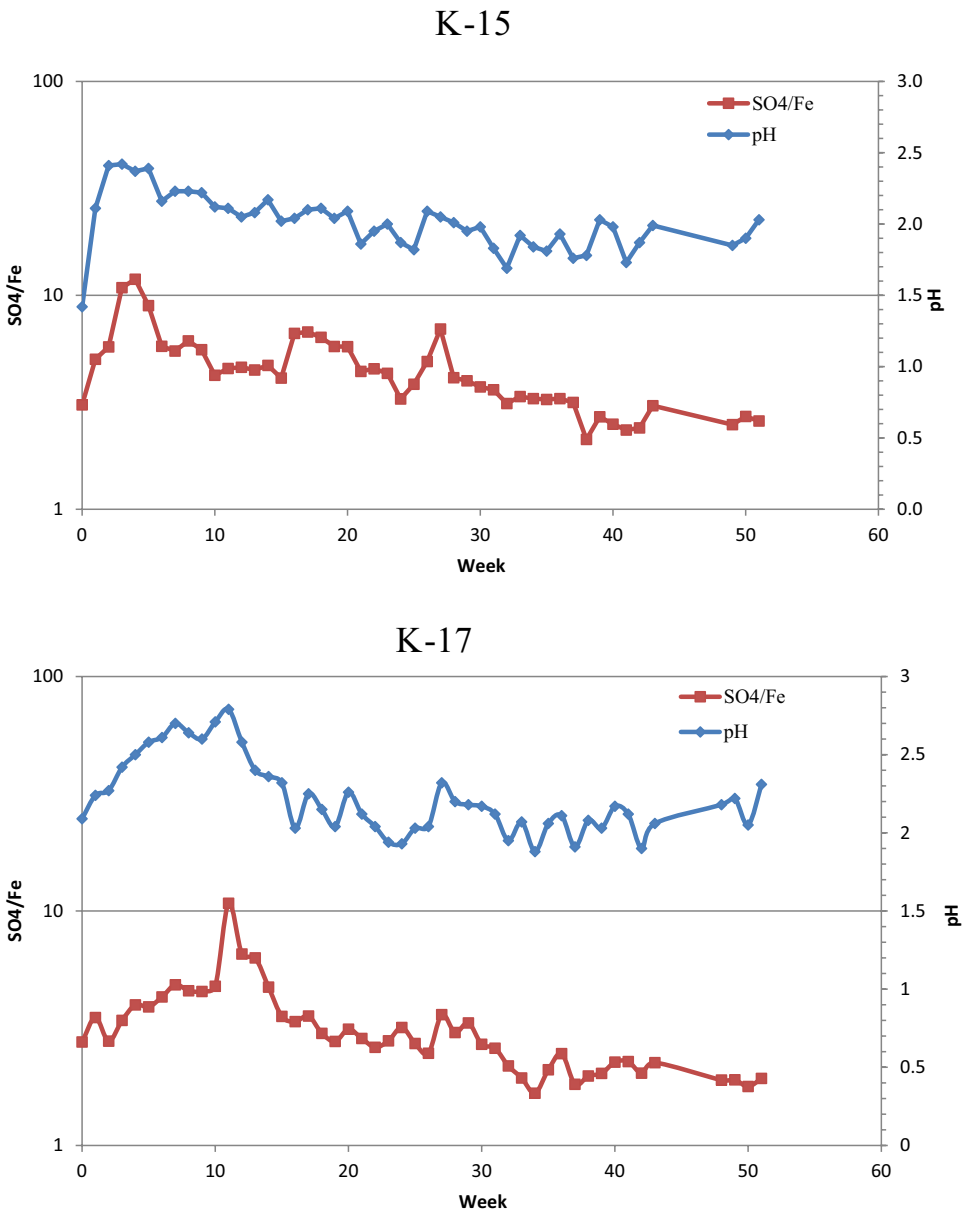

Fig. 14 Variations observed in SO4/Fe molar ratio of weekly eluents obtained from humidity cell tests

Supplementary Information The online version contains supplementary material available at https://doi.org/10.1007/s10230-023-00956-0.

Acknowledgements This research was supported by a grant 110Y235 provided by the Scientific and Technological Research Council of Turkey (TÜBITAK). We thank the anonymous reviewers for their constructive and detailed comments.

Data availability All data were already given in paper.

References

ASTM (2001) Standard test method for accelerated weathering of solid materials using a modified humidity cell. American Society for Testing and Materials, Cham, pp 5744–5796

AWWA (1995) Standard methods for the examination of water and wastewater, 19th edn. American Water Works Association, Washington

Bethke CM (1998) The geochemist's workbench release 3.0. A users guide to Rxn, Act2, React, and Gtplot, Univ of Illinois, Urbana

Carbone C, Dinelli E, Marescotti P, Gasparotto G, Lucchetti G (2013) The role of AMD secondary minerals in controlling environmental pollution: indications from bulk leaching tests. J Geochem Explor 132:188–200

Çiftçi E, Yalçınalp B, Housh TB (2009) Ore mineralogy, Cu-S-Pb isotope- and base-precious metal geochemistry of the eastern Pontides volcanogenic massive sulfide deposits. In: Proceedings of 2nd International Symp on the Geology of the Black Sea Region, Ankara, p 44

De Choudens-Sanchez V, Gonzalez LA (2009) Calcite and aragonite precipitation under controlled instantaneous supersaturation: elucidating the role of $CaCO_3$ saturation state and Mg/Ca ratio on calcium carbonate polymorphism. J Sediment Res 79(6):363–376

Dold B (2014) Evolution of acid mine drainage formation in sulphidic mine tailings. Minerals 4:621–641. https://doi.org/10.3390/min4030621

EPA (2007) Microwave assisted acid digestion of aqueous samples and extracts (EPA Method 3015A).

Hammarstrom JM, Seal RR, Meier AL, Kornfeld JM (2005) Secondary sulfate minerals associated with acid drainage in the eastern US: recycling of metals and acidity in surface environments. Chem Geol 215:407–431

Jacobs JA, Lehr JH, Testa SM (2014) Acid mine drainage, rock drainage, and acid sulfate soils: causes, assessment, prediction, prevention, and remediation. Wiley, Hoboken

Jambor JL, Nordstrom DK, Alpers CN (2000) Metal-sulfate salts from sulfide mineral oxidation. Rev Min Geochem 40:302–350

Kraeff A (1963) Geology and mineral deposits of the Hopa-Murgul region (western part of the province of Artvin, Turkey). MTA Bull 60:45–60

Lapakko K (2002) Metal mine rock and waste characterization tools: an overview. Mining, Minerals, and Sustainable Development (MMSD) working paper, 67. https://www.iied.org/g00559

Lottermoser B (2007) Mine wastes: characterization, treatment and environmental impacts. Springer

Miller FP, Vandome AF, McBrewster J (2009) Acid mine drainage. Alphascript Publishing, Aurora

Nordstrom DK (1982) Aqueous pyrite oxidation and the consequent formation of secondary iron minerals. In: Kittrick JA, Fanning DS, Hossner LR (eds) Acid sulfate weathering. Soil Science Society of America, pp 37–56

Nordstrom DK, Alpers CN (1999) Geochemistry of acid mine waters. In: Plumlee GS, Logsdon MJ (eds) The environmental geochemistry of mineral deposits, reviews in economic geology, 6th edn. Springer, pp 133–160

Simonovic R (1972) Report on geological 1:10000 mapping and prospecting in the Artvin area (Kuarshane, Sinkot, Irsa, Seyitli-Umasen), M.T.A. General Directory, Report 4912, Ankara, Turkey

Singer PC, Stumm W (1970) Acidic mine drainage: the rate-determining step. Science 167:1121–1123

Sunagawa I, Takahashi Y, Imai H (2007) Strontium and aragonite-calcite precipitation. J Miner Pet Sci 102(3):174–181

TÜBİTAK (2014) Geochemical processes controlling the generation and environmental impacts of acid mine drainage in the case of polymetallic mines, Artvin. Project 110Y235, Final report (**in Turkish**)

Van A (1990) Geochemistry, petrogenesis and massive sulfide mineralizations of the Artvin Region in the Pontide Belt. PhD Diss, Turkey Black Sea Tech Univ (**in Turkish**)

Zeller EJ, Wray JL (1956) Factors influencing precipitation of calcium carbonate. AAPG Bull 40(1):140–152